Journal of African Earth Sciences 197 (2023) 104750

Contents lists available at ScienceDirect

Journal of African Earth Sciences

journal homepage: www.elsevier.com/locate/jafrearsci

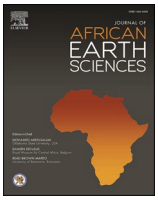

The timing and tectonic context of Pan-African gem bearing pegmatites in Malawi: Evidence from Rb–Sr and U–Pb geochronology

Tuhin Chakraborty [a,*], Charles F. Kankuzi [a,b], Johannes Glodny [c], Dirk Frei [d], Steffen H. Büttner [a]

[a] Department of Geology, Rhodes University, Grahamstown, 6140, Eastern Cape, South Africa
[b] Geology and Earth Sciences Department, University of Malawi, Zomba, Malawi
[c] GFZ German Research Centre for Geosciences, Potsdam, Germany
[d] Department of Earth Science, University of Western Cape, South Africa

ARTICLE INFO

Keywords:
Malawi
Pegmatite
Gondwana
East Africa orogen
Kuunga
Rb–Sr
U–Pb zircon

ABSTRACT

The Pan-African belts of Malawi contain a largely unexplored endowment of gem bearing pegmatites. We present U–Pb in zircon (LA-ICPMS) and Rb–Sr mineral isochron geochronological and isotope data from pegmatites across Malawi. The pegmatites contain tourmaline, beryl, aquamarine, zircon, amethyst and sunstone as gemstone species. Two zircon bearing pegmatites in southern Malawi intruded early in the Pan-African orogenic cycle at 719 ± 5 Ma and 729 ± 4 Ma and are associated with the emplacement of alkaline rocks that formed during an intra-continental rifting episode in the eastern part of former Rodinia. One further zircon pegmatite containing inherited zircon of a similar age (746 ± 44 Ma) was emplaced at 598 ± 15 Ma, after the assembly of Western and Eastern Gondwana and the formation of the East African Orogen (EAO). The majority of the analysed pegmatites, however, are significantly younger. The ~550 Ma pegmatites were emplaced during the Kuunga Orogeny, correlating with the collision of northern and southern Gondwana cratonic entities. During a prolonged post-collisional period, possibly related to crustal collapse and extension, further gem-mineralised pegmatites formed at ~520 ± 6 Ma and ~500–485 Ma. The youngest pegmatite intruded in the southern Malawian Ntcheu area in the Middle Ordovician at ~460 Ma. A large spread in $^{87}Sr/^{86}Sr$ initial isotopic ratios between 0.70556 and 0.79018 suggests a variety of magma sources for the Kuunga-related pegmatites with a variably strong crustal affinity.

1. Introduction

The Pan-African belts in eastern and southeastern Africa formed over a prolonged period of contractional, transcurrent and collisional tectonics in the late Neoproterozoic and early Paleozoic. Two major orogenic belts formed during this time, the East African Orogen (EAO), stretching from today's Arabic Peninsula to Malawi and Mozambique, and the slightly younger Kuunga Orogen, transecting southern Africa from east to west, from northern Mozambique through Malawi, Zambia, Botswana and Namibia (e.g., Stern, 1994; Grantham et al., 2003, 2008, 2019; Meert, 2003; Oriolo et al., 2017, Fig. 1).

In present-day southern and eastern Africa, the amalgamation of Gondwana during the East African and Kuunga orogenies followed the subduction of the Mozambique Ocean and its western extension, the Khomas Ocean, that formed an oceanic connection to the Adamastor Ocean (Meert, 2003; Oriolo et al., 2017, 2021, Fig. 1). These oceans had existed since the early stages of Rodinia break-up in the Neoproterozoic (~850–800 Ma; Meert, 2003; Li et al., 2008), forming complex marginal basins and intra-oceanic magmatic arcs that were active between ~800 and 700 Ma (e.g. Stern, 1994; Meert, 2003; Grantham et al., 2003; Collins and Pisarevsky, 2005; Fitzsimons and Hulscher, 2005; Jöns and Schenk, 2008). From about 700 Ma onwards the oceanic basins closed, leading to the collisional assembly of Gondwana between ~650 and 520 Ma, with an extended post-collisional and possibly post-Pan-African period of deformation, metamorphism and magmatic activity in the EAO and the Kuunga Orogen, lasting to the end of the Ordovician (e.g. Grantham et al., 2003, 2008; Meert, 2003; Oriolo et al., 2017, 2021). In this paper we refer to the evolution of related lithospheric entities from the break-up of Rodinia, through the stages of oceanic growth and consumption to the collisional assembly of Gondwana during the East African and Kuunga orogenies as the Pan-African orogenic cycle.

The region of Malawi and parts of the neighbouring Mozambique,

* Corresponding author.
E-mail address: t.chakraborty@ru.ac.za (T. Chakraborty).

https://doi.org/10.1016/j.jafrearsci.2022.104750
Received 9 March 2022; Received in revised form 4 October 2022; Accepted 4 October 2022
Available online 7 October 2022
1464-343X/

Tanzania and Zambia are located at the intersection of the southern part of the EAO, known as the Mozambique Belt, and the Kuunga Orogen (Fig. 1). The EAO, created by the collision of Western and Eastern Gondwana, formed mainly between ~690 and 600 Ma, following the subduction and accretion of the Mozambique Ocean and related magmatic arcs (e.g. Grantham et al., 2003, 2013; Meert, 2003; Oriolo et al., 2017; Fritz et al., 2013). The Kuunga Orogeny (~580–520 Ma) is somewhat younger (Meert, 2003), although, arguably, EAO tectonics, magmatism and metamorphism may have outlasted the main collision phase in some places, overlapping with the Kuunga Orogeny in time. The Kuunga Orogen formed following the consumption of the Khomas Ocean along the boundary of southern cratonic blocks (Kalahari Craton, Dronning Maud Land/Antarctica) and northern ones (Congo Craton, India) (Meert, 2003; Oriolo et al., 2017). This formed the Damara, Zambezi and Lurio belts, and significant large-scale shear zones, such as the Mwembeshi shear zone that extends from central Malawi westwards into Zambia towards the Lufilian Arc (e.g., Lawver et al., 1998; Meert, 2003; Grantham et al., 2003, 2008, 2013; Reeves et al., 2004; Viola et al., 2008; Fitzsimons, 2016) (Fig. 1). Locally, the Kuunga Orogeny also led to transcurrent shearing along the EAO further north, overprinting or reactivating older structures and rocks between ~550 and 520 Ma (Meert, 2003; Grantham et al., 2013).

During the Pan-African Wilson cycle from Rodinia break-up to the collisional assembly of Gondwana the lithosphere in south-eastern Africa was exposed to several episodes of conditions suitable to the formation of granitic magmas. While some Malawian granites were dated in earlier studies (e.g. Kröner et al., 2001), little is known about the magma sources, tectonic affiliation, context, and mineralization of granitic pegmatites in Malawi (Holt, 1965; Gaskell, 1973). Because of their economic potential for Malawi, the current study's focus is on gem bearing Pan-African pegmatites, which contain tourmaline, zircon, beryl, aquamarine, amethyst, and sunstone. We present Rb–Sr mineral isochrons and U–Pb zircon data to establish the chronological framework of ten such pegmatites (online supplement 1). The $^{87}Sr/^{86}Sr$ initial ratios derived from mineral isochron data for the pegmatites are used to identify the possible magma sources of these pegmatites. Our results

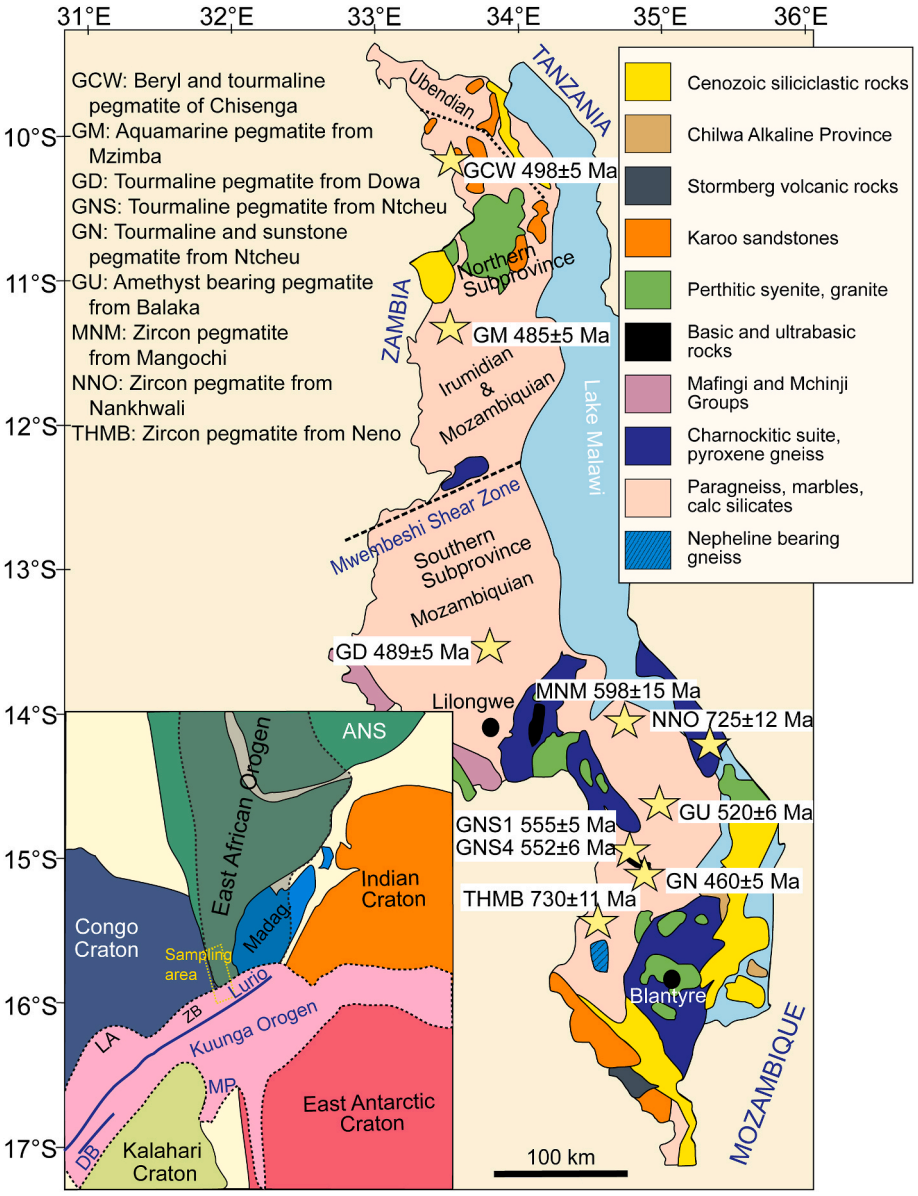

Fig. 1. Simplified geology of Malawi with sample locations and emplacement ages of gem bearing pegmatites (modified after Carter and Bennet, 1973; Dill, 2007). Inset. Major cratonic entities after the assembly of Gondwana during the East African and Kuunga orogenies (modified after Meert, 2003). DB: Damara Belt; LA: Lufilian Arc; ZB: Zambesi Belt; ANS: Arabian-Nubian Shield.

show several episodes of pegmatite formation spanning ~270 million years, from the rifting of former Rodinia lithosphere to the prolonged period of Gondwana assembly and to late/post-Pan-African pegmatites of Ordovician age.

2. Regional geology

2.1. Malawi

Modern geological mapping of Malawi has been undertaken by a consortium of geological surveys under the leadership of the French Geological Survey BRGM since 2017, but the results are not yet publicly available. Hence, we use the traditional and up to now widely used lithostratigraphic subdivision (Carter and Bennet, 1973) to put the pegmatite occurrences into their geological context.

The Precambrian to the early Palaeozoic rocks are commonly referred to as the Malawi Basement Complex (Carter and Bennet, 1973). This Basement Complex, subdivided into the Northern and Southern Sub-provinces, comprises gneisses, schists, and granulites with associated mafic, ultramafic, syenitic and granitic rocks (Bloomfield, 1968), which formed or were overprinted during the Ubendian, the Irumide and the Pan-African orogenic phases. The south-eastern end of the Palaeoproterozoic Ubendian Belt crosses through northernmost Malawi (Fig. 1; Ray, 1974), bordering the Meso-to Neoproterozoic Irumide Belt further south.

Early in the Pan-African orogenic cycle, alkaline magmatic rocks, such as the Tambani complex and the North Nyasa Alkaline Province formed between ~710 and ~750 Ma (Cooper and Bloomfield, 1961; Lenoir et al., 1994; Eby et al., 1998; Hanson, 2003; Ashwal et al., 2007). Ashwal et al. (2007) proposed rifting in the Rodinia lithosphere as the tectonic setting at that time. Together with their Paleo-to Mesoproterozoic host rocks, these alkaline bodies were intensely reworked during the collisional episodes that formed the East African and Kuunga Orogens (Carter and Bennet, 1973; Kröner et al., 2001). Grantham et al. (2013) considers the Mesoproterozoic basement in central and southern Malawi as part of the Namuno Terrane, a part of the East African Orogen that overrides the Nampula Terrane in the south and southeast (northern Mozambique) during the Kuunga Orogeny (~580–540 Ma). The collision formed complex contractional and transpressional structures. The Lurio Belt (Fig. 1), extending from Mozambique through southernmost Malawi, is the most prominent of these structures. High-grade metamorphism and magmatism related to the Kuunga collision between 580 and 540 Ma (Kröner et al., 2001; Grantham et al., 2013) was followed by crustal extension and late granite and pegmatite emplacement between ~540 and ~515 Ma, and possibly continuing to 490 Ma (Viola et al., 2008; Ueda et al., 2012; Grantham et al., 2013).

Most of the samples pegmatites come from the Southern Subprovince (Fig. 1), or, according to Grantham et al. (2013), the Malawian part of the Namuno Terrane. Their host rocks consist of medium-to high-grade paragneisses, granulites and hornblende-biotite gneiss interlayered with sillimanite-garnet metapelites (Kröner et al., 2001), underlain by banded two pyroxene granulites and tonalite-trondhjemite-granodiorite (TTG) gneisses and charnockites (Kröner et al., 2001; Tsunogae et al., 2021).

2.2. Gem bearing pegmatites in Malawi and neighbouring countries

A large proportion of the world's gem-producing pegmatites are found in Gondwana and formed during the Pan-African orogenic cycle (870–550 Ma; Simmons et al., 2012). Major gem bearing pegmatites were reported from Mozambique, Tanzania, Zambia, Madagascar, and Kenya (Simmons et al., 2012). Pan-African pegmatites hosted in the granulite-facies basement in the Ubendian and Usagaran Belts of Tanzania contain ruby, sapphire and emerald, and these belts extend to northern Malawi (McConnell, 1950; Sutton et al., 1954; Smirmov et al., 1973; Harris, 1981; Sommer and Kröner, 2019; Ganbat et al., 2021). The eastern Irumide orogenic belt in Zambia hosts Pan-African granitic beryl bearing pegmatite swarms (Foster, 1965; Daly, 1986; Klerkx et al., 1998; Carranza et al., 2005), and also this belt extends into northern Malawi. Another example is the occurrence of Alto Ligonha pegmatites (Neiva, 2013), formed in the Nampula Terrane of northern Mozambique around ~ 600–550 Ma. The Nampula Terrane forms the tectonic footwall of the Namuno Terrane in southern Malawi since the Kuunga collision at about 580–540 Ma (Grantham et al., 2013). Furthermore, a wide variety of gemstone deposits are densely scattered along the Mozambique Belt through the neighbouring countries of Mozambique, Tanzania and Zambia, yielding spectacular occurrences of gemstones such as sapphire, ruby, emerald, tourmaline as well as beryl varieties (Malisa and Muhongo, 1990; Muhongo, 1999; Simonet et al., 2000; Simmons et al., 2012). Despite this abundance of gemstone-mineralised pegmatites in the Mozambique Belt of the neighbouring countries, Malawi has not received much attention in related mineral exploration and research.

3. Analytical techniques

In order to associate pegmatite emplacement with specific episodes of the tectono-metamorphic evolution of Malawi, we selected ten pegmatites for geochronological work (online supplement 1; Fig. 1). Three pegmatites (MNM, NNO, THMB; Figs. 2 and 3) contain large (~5–35 mm) gem quality zircon crystals that formed during pegmatite crystallization. These pegmatites were dated using U–Pb isotope analysis which was carried out using SF-LA-ICP-MS analysis at Stellenbosch University. In other pegmatites, zircon may be present as small crystals but with equivocal provenance (parent granite, source rock). These pegmatites (GCW, GM1, GD, GNS-1, GNS-4, GU, GN; Figs. 2 and 3) contain alkali feldspar, plagioclase, muscovite and ±biotite assemblages suitable for Rb–Sr mineral isochron geochronology using thermal ionization mass spectrometry (TIMS). In addition to the emplacement age, Rb–Sr mineral isochrons deliver the initial strontium isotope compositions of the melt. These analyses were made at the German Research Centre for Geoscience (GFZ) in Potsdam. Details of the analytical techniques can be found in the online supplementary material 2. The Rb–Sr isotope ratios and ages and zircon U–Pb isotope ratios and ages are listed in Tables 1 and 2 respectively.

4. Results

4.1. Sample description

4.1.1. Beryl and tourmaline bearing pegmatites of Chitipa: GCW

The beryl and tourmaline bearing pegmatite GCW is hosted in the cordierite-sillimanite gneiss and is collected from Chitipa in northern Malawi (Fig. 1). These pegmatites are poorly exposed and comprehensive detail about their internal features could not be obtained from field observations. The principal mineral assemblage is muscovite + K-feldspar + quartz + beryl + plagioclase + tourmaline, with occasional presence of garnet and tantalite. In thin section, the mineral assemblage does not show evidence of significant alteration (Fig. 4a).

4.1.2. Aquamarine bearing pegmatites of Kafukule and Luhomero–Mzimba: GM

This aquamarine bearing pegmatite from the Mzimba district (Figs. 1 and 2b) intruded into amphibolite facies banded sillimanite-garnet-biotite basement gneisses, granite, and syenite. Although located 120 km further north (Fig. 1), the GM pegmatite was emplaced in similar host rocks as GCW. The contacts between the pegmatite and the host rocks are sharp (Fig. 3a) and the pegmatite does not show any macroscopic evidence of deformation. An earlier study by Graziani et al. (1983) proposed an emplacement pressure of 4 kbar and a temperature of 430–650 °C, corresponding to a depth of about 15 km. The minerals present in this pegmatite are muscovite, K-feldspar, plagioclase and aquamarine. The assemblage shows no evidence of later alterations.

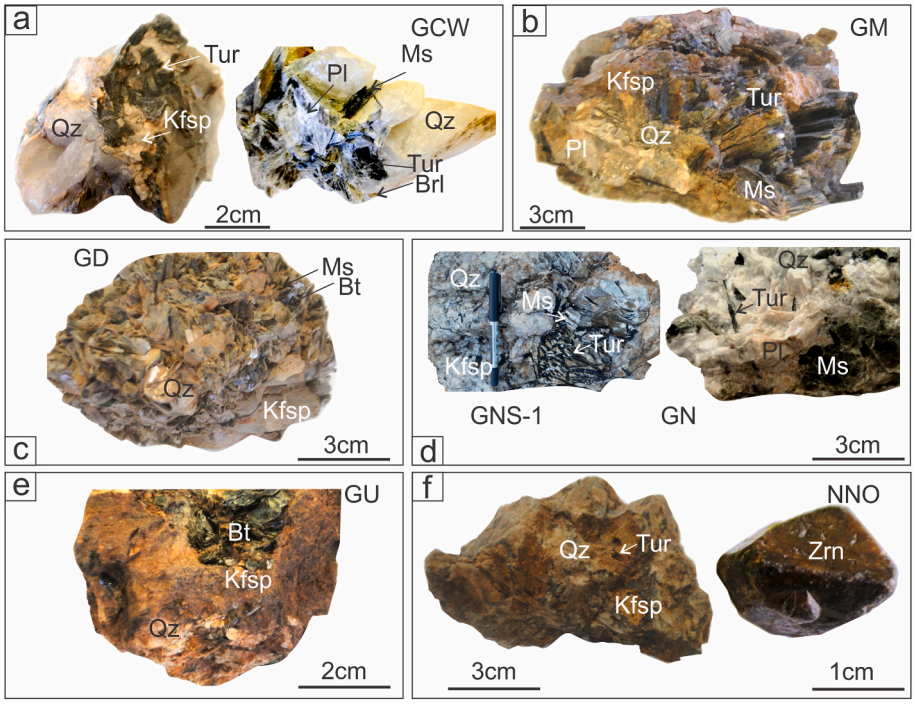

Fig. 2. (a–f) Representative hand specimens from pegmatites. Mineral abbreviations after Whitney and Evans (2010); Brl: beryl, Tur: tourmaline, Qz: quartz, Fsp: feldspar, Kfs: K-feldspar; Ms: muscovite, Bt: biotite, Zrn: zircon, Pl: plagioclase.

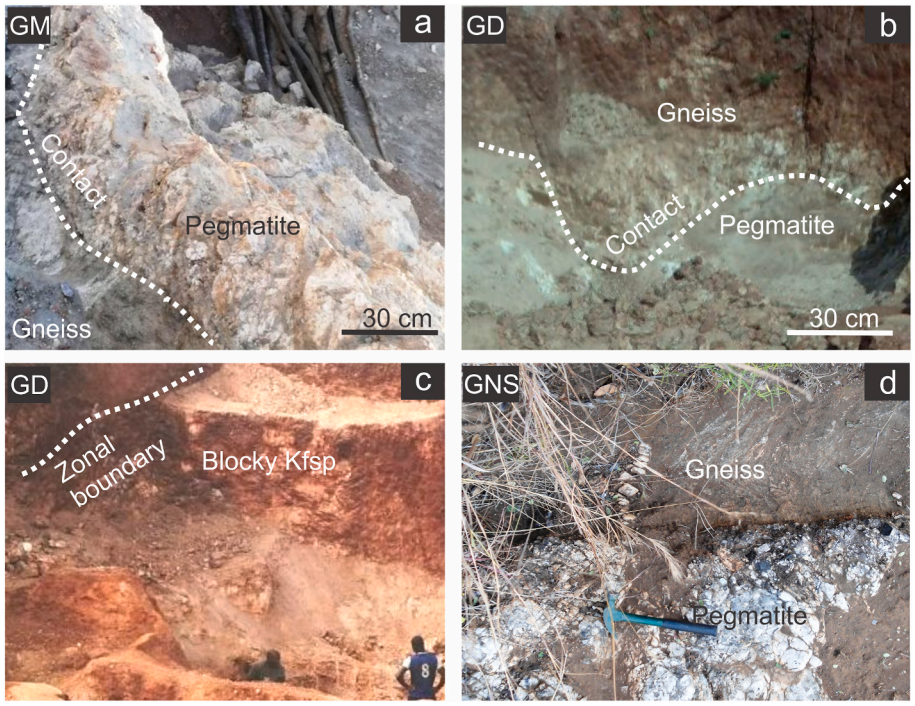

Fig. 3. (a–d) Typical field appearance and relations of pegmatites with their country rocks. a) Sharp contact of GM pegmatites with host rocks; b) GD pegmatite from Dowa showing a sharp contact with the host gneisses; c) Blocky feldspar in the GD pegmatite; d) Sharp contact between the pegmatite from Ntcheu (GNS) and the host gneiss.

Large and randomly oriented pegmatitic muscovite may show undulose extinction but is otherwise undeformed (Fig. 4c).

4.1.3. Tourmaline bearing pegmatites of Dowa: GD

This tourmaline bearing pegmatite sample was collected from the Dowa area in the central region of Malawi (Figs. 1, 2c and 4d). The pegmatites intruded into the garnet bearing sillimanite-biotite-hornblende gneisses and consist of K-feldspar, plagioclase, tourmaline, muscovite and quartz as the principal constituents. The pegmatites show a compositional zonation from a quartz-feldspar dominated core zone to a more mica-tourmaline-rich wall zone (Fig. 3c). These pegmatites are macroscopically undeformed and show sharp contacts with the host

Table 1
Rb–Sr isotope ratios and ages of minerals in pegmatites from Malawi.

Sample No.	Material	Rb [ppm]	Sr [ppm]	87Rb/86Sr	87Sr/86Sr	87Sr/86Sr 2σm [%]
GCW (498.4 ± 5.2 Ma; MSWD = 1.7, Sri = 0.790177 ± 0.000053)						
	Muscovite2	1400	7.13	941	7.412003	0.001
	Muscovite1	1375	7.73	797	6.320319	0.002
	Plagioclase	13.4	137	0.286	0.792172	0.0021
GM (485.1 ± 4.8 Ma; MSWD = 1.03, Sri = 0.7762 ± 0.0012)						
	Muscovite 2	835	5.15	690	5.496292	0.001
	Muscovite 1	874	4.87	797	6.182156	0.0009
	K-feldspar	163	22.8	21.2	0.919024	0.0033
	Plagioclase	53.8	16.5	9.54	0.841344	0.008
GD (489.0 ± 5.1 Ma; MSWD = 0.41, Sri = 0.7405 ± 0.0048)						
	K-feldspar	235	18.3	38.1	1.001654	0.0023
	Muscovite 2	984	2.66	3850	27.22056	0.0017
	Muscovite 1	974	2.64	3751	26.37325	0.002
GNS-1 (555.4 ± 4.7 Ma; MSWD = 2.0, Sri = 0.706067 ± 0.000035)						
	Muscovite 1	471	8.24	189	2.158278	0.0013
	Muscovite 2	297	16.7	53.5	1.124887	0.0041
	K-feldspar	377	161	6.82	0.759585	0.0011
	Plagioclase	1.41	273	0.015	0.706183	0.002
GNS-4 (552.4 ± 6.0 Ma; MSWD = 0.14, Sri = 0.70558 ± 0.00062)						
	Muscovite 1	380	12.3	96.4	1.454274	0.0021
	K-feldspar	297	204	4.22	0.738285	0.0016
	Muscovite 2	442	14.6	94	1.432295	0.0011
GN (459.6 ± 5.2 Ma; MSWD = 0.03, Sri = 0.7893 ± 0.0099)						
	K-feldspar	1300	49.8	79.9	1.30403	0.0011
	Muscovite 2	1524	7.17	1010	7.291396	0.0012
	Muscovite 1	1609	6.34	1380	9.68707	0.004
GU (520.4 ± 5.5 Ma; MSWD = 3.3, Sri = 0.718733 ± 0.000059)						
	K-feldspar	835	142	17.3	0.843494	0.0014
	Plagioclase	21.2	171	0.358	0.721346	0.0017
	Biotite	488	7.34	224	2.364989	0.001

rocks (Fig. 3b).

4.1.4. Tourmaline bearing pegmatite from Ntcheu: GNS-1, GNS-4

This tourmaline bearing pegmatite from the Ntcheu-Balaka area (Figs. 1 and 2d) is hosted in Mesoproterozoic gneiss. The contact between the pegmatite and the host gneiss is sharp (Fig. 3d) but locally intense tourmalinization in the hosting gneiss suggests pegmatitic fluid extraction along the contact. The pegmatites consist of muscovite, K-feldspar, plagioclase and tourmaline. Except for undulose extinction in quartz (Fig. 4e) the pegmatite is undeformed. The GNS-1 pegmatite intruded into granular banded garnet-hornblende-diopside gneiss (Walshaw, 1965), whereas GNS-4 intruded into hornblende-biotite-gneiss. The pegmatites have variably concordant to discordant relationships with their host rocks.

4.1.5. Tourmaline and sunstone bearing pegmatite from Ntcheu: GN

The tourmaline and sunstone bearing pegmatite GN is collected from the Ntcheu district (Fig. 1), about 10 km southeast of the GNS pegmatites. The GN pegmatite is hosted in hornblende-biotite gneiss and is discordant to the main fabric of the hosting gneiss, with which it shows sharp contacts. The principal mineral assemblage is K-feldspar, muscovite, quartz, and gem-quality tourmaline and sunstone (Fig. 2d). No macroscopic deformation is evident. The mineral assemblage is unaltered and forms a primary igneous texture (Fig. 4f).

4.1.6. Amethyst bearing pegmatite from Balaka: GU

The amethyst bearing pegmatite is sampled from the Balaka district (Fig. 1). The pegmatite is hosted in Mesoproterozoic granulite and biotite garnet gneiss of the Basement Complex (Bloomfield and Garson, 1965). The pegmatite is discordant to the hosting biotite-garnet gneiss and forms a sharp contact. Mineralogically these pegmatites consist of biotite, K-feldspar, quartz/amethyst (Fig. 2e), plagioclase, and minor amounts of garnet, ilmenite and monazite.

4.1.7. Zircon bearing pegmatite from Nankhwali-Mangochi: MNM and NNO

The pegmatites MNM and NNO are hosted in gneisses and two-pyroxene granulite near Cape Maclear and Uzuzu in Mangochi (Fig. 1). Along with the pegmatites, a swarm of microgranite and microsyenite dykes were emplaced (King and Dawson, 1976). The mineral assemblage of the MNM pegmatite consists of K-feldspar, biotite, quartz, and zircon with accessory sphene and monazite, whereas the NNO pegmatites are composed of K-feldspar, quartz, muscovite and tourmaline with accessory zircon, garnet, and ilmenite (Fig. 2f). A gradual decrease in the grain size is observed from the core part of the pegmatites to the margin. The sub-vertical pegmatite dykes are un-deformed. Some are concordant and others discordant to the main fabric of the host rocks.

4.1.8. Zircon pegmatite from Neno: THMB

The THMB pegmatite from Neno, southern Malawi (Fig. 1) was emplaced into hornblende biotite gneiss. The host rocks and pegmatites are largely covered by regolith, obscuring much of the field relationships. The pegmatites are concordant with the gneissosity in their host, and do not show evidence of deformation. The contact between the pegmatites and host rock gneisses is sharp. The THMB pegmatites are composed of coarse-grained K-feldspar, quartz, apatite, amphibole, zircon, biotite and ilmenite. The texture reveals a graphic intergrowth of coarse-grained minerals. Gem-quality zircon reaches up to 35 mm in size and is generally euhedral. The sampling site is approximately 10 km north of the Tambani alkaline complex (Fig. 1).

4.2. Rb–Sr geochronology

4.2.1. Beryl-tourmaline pegmatite: sample GCW

The Rb–Sr isochron defined by plagioclase and two separate undeformed muscovite crystals yields a late Pan-African age of 498 ± 5 Ma with a reasonably low MSWD (mean squared weighted deviation) of 1.7 (Fig. 5a; Table 1). The initial $^{87}Sr/^{86}Sr$ ratio of 0.790177 ± 0.000053 (Table 1) is very high, even for melts derived from crustal sources

Table 2
U–Pb isotope ratios and ages of zircons in pegmatites from Malawi.

MNM (pegmatites from the Nankhwali-Mangochi)

			Ratios							Ages (Ma)						
S no.	**U [ppm]**	**Pb [ppm]**	**207 Pb/ 235U**	**±2σ**	**206 Pb/ 238U**	**±2σ**	**rho**	**207Pb/ 206 Pb**	**±2σ**	**207 Pb/ 235U**	**±2σ**	**206 Pb/ 238U**	**±2σ**	**207Pb/ 206 Pb**	**±2σ**	**concordance (%)**
1	25	2	0.8035	0.0345	0.0974	0.0022	0.53	0.0598	0.0022	599	26	599	14	597	79	100
2	24	2	0.8032	0.0347	0.0970	0.0022	0.53	0.0600	0.0022	599	26	597	14	605	79	99
3	28	3	0.7987	0.0359	0.0970	0.0022	0.50	0.0597	0.0023	596	27	597	14	593	84	101
4	26	2	0.7922	0.0333	0.0966	0.0022	0.54	0.0595	0.0021	592	25	594	14	585	77	102
5	24	2	0.7768	0.0354	0.0934	0.0021	0.50	0.0603	0.0024	584	27	576	13	615	85	94
6	29	3	0.7911	0.0330	0.0964	0.0022	0.55	0.0595	0.0021	592	25	593	14	587	76	101
7	150	18	1.0687	0.0385	0.1205	0.0026	0.61	0.0643	0.0018	738	27	733	16	753	60	97
8	153	18	1.0600	0.0401	0.1203	0.0026	0.58	0.0639	0.0020	734	28	732	16	739	66	99
9	59	6	0.8001	0.0345	0.0960	0.0021	0.51	0.0604	0.0022	597	26	591	13	619	80	96
10	54	5	0.7974	0.0295	0.0967	0.0022	0.60	0.0598	0.0018	595	22	595	13	597	64	100
11	23	2	0.8014	0.0374	0.0963	0.0022	0.50	0.0603	0.0024	598	28	593	14	616	87	96
12	23	2	0.7641	0.0342	0.0929	0.0021	0.51	0.0596	0.0023	576	26	573	13	591	84	97
13	27	3	0.8050	0.0338	0.0970	0.0022	0.55	0.0602	0.0021	600	25	597	14	611	76	98
14	26	2	0.7895	0.0361	0.0958	0.0022	0.50	0.0598	0.0024	591	27	590	14	596	86	99
15	22	2	0.7939	0.0349	0.0963	0.0022	0.52	0.0598	0.0022	593	26	592	14	597	81	99
16	25	2	0.8066	0.0369	0.0982	0.0022	0.50	0.0596	0.0024	601	27	604	14	588	86	103
17	23	2	0.7959	0.0341	0.0967	0.0022	0.54	0.0597	0.0022	595	25	595	14	592	78	100
18	25	2	0.7828	0.0338	0.0953	0.0022	0.53	0.0596	0.0022	587	25	587	13	589	79	100
19	23	2	0.7990	0.0351	0.0972	0.0023	0.53	0.0596	0.0022	596	26	598	14	589	81	102
20	25	2	0.7964	0.0406	0.0968	0.0022	0.45	0.0597	0.0027	595	30	596	14	592	99	101
21	23	2	0.7921	0.0360	0.0960	0.0022	0.51	0.0599	0.0023	592	27	591	14	599	85	99

NNO (pegmatites from the Nankhwali-Mangochi)

			Ratios							Ages (Ma)						
S no.	U [ppm]	Pb [ppm]	207 Pb/ 235U	±2σ	206 Pb/ 238U	±2σ	rho	207Pb/ 206 Pb	±2σ	207 Pb/ 235U	±2σ	206 Pb/ 238U	±2σ	207Pb/ 206 Pb	±2σ	concordance (%)
1	466	55	1.0332	0.0315	0.1183	0.0026	0.71	0.0634	0.0014	721	22	721	16	720	46	100
2	615	72	1.0268	0.0323	0.1177	0.0026	0.69	0.0633	0.0014	717	23	717	16	717	48	100
3	382	46	1.0410	0.0319	0.1194	0.0026	0.71	0.0632	0.0014	724	22	727	16	716	46	102
4	394	47	1.0391	0.0319	0.1192	0.0026	0.70	0.0633	0.0014	723	22	726	16	717	46	101
5	373	44	1.0447	0.0329	0.1194	0.0026	0.69	0.0635	0.0014	726	23	727	16	723	48	101
6	480	57	1.0355	0.0315	0.1187	0.0026	0.71	0.0633	0.0014	722	22	723	16	717	46	101
7	452	51	0.9879	0.0302	0.1136	0.0025	0.71	0.0631	0.0014	698	21	693	15	712	46	97
8	431	49	0.9819	0.0302	0.1129	0.0024	0.70	0.0631	0.0014	695	21	690	15	711	47	97
9	385	46	1.0567	0.0326	0.1201	0.0026	0.70	0.0638	0.0014	732	23	731	16	736	46	99
10	450	54	1.0522	0.0324	0.1199	0.0026	0.70	0.0637	0.0014	730	22	730	16	731	47	100
11	434	52	1.0564	0.0324	0.1203	0.0026	0.70	0.0637	0.0014	732	22	733	16	731	47	100
12	404	48	1.0406	0.0323	0.1190	0.0026	0.69	0.0634	0.0014	724	22	725	16	722	48	100
13	320	38	1.0557	0.0334	0.1197	0.0026	0.68	0.0640	0.0015	732	23	729	16	740	49	99
14	190	22	1.0012	0.0358	0.1139	0.0025	0.61	0.0637	0.0018	704	25	695	15	733	60	95
15	41	5	1.0548	0.0393	0.1199	0.0026	0.59	0.0638	0.0019	731	27	730	16	736	64	99
16	78	9	1.0317	0.0394	0.1180	0.0026	0.58	0.0634	0.0020	720	28	719	16	722	66	100
17	43	5	1.0401	0.0414	0.1185	0.0026	0.56	0.0637	0.0021	724	29	722	16	730	70	99
18	208	25	1.0475	0.0356	0.1183	0.0026	0.64	0.0642	0.0017	728	25	721	16	749	55	96

THMB (pegmatites from the Neno)

			Ratios							Ages (Ma)						
S no.	U [ppm]	Pb [ppm]	207 Pb/ 235U	±2σ	206 Pb/ 238U	±2σ	rho	207Pb/ 206 Pb	±2σ	207 Pb/ 235U	±2σ	206 Pb/ 238U	±2σ	207Pb/ 206 Pb	±2σ	concordance (%)
1	594	72	1.0647	0.0315	0.1210	0.0024	0.67	0.0638	0.0014	736	22	736	15	736	46	100
2	835	101	1.0499	0.0335	0.1205	0.0024	0.62	0.0632	0.0016	729	23	733	14	716	53	102
3	120	14	1.0442	0.0347	0.1186	0.0024	0.60	0.0639	0.0017	726	24	722	14	738	56	98
4	790	93	1.0390	0.0315	0.1183	0.0023	0.65	0.0637	0.0015	723	22	721	14	732	49	98
5	897	108	1.0611	0.0379	0.1203	0.0024	0.55	0.0640	0.0019	734	26	732	14	740	63	99
6	1100	132	1.0479	0.0319	0.1201	0.0024	0.65	0.0633	0.0015	728	22	731	14	718	49	102
7	714	85	1.0309	0.0314	0.1186	0.0023	0.65	0.0630	0.0015	719	22	723	14	709	49	102
8	800	96	1.0582	0.0328	0.1205	0.0024	0.64	0.0637	0.0015	733	23	733	14	732	51	100
9	680	83	1.0714	0.0319	0.1219	0.0024	0.66	0.0638	0.0014	739	22	741	15	734	47	101
10	739	87	1.0237	0.0319	0.1177	0.0023	0.63	0.0631	0.0015	716	22	717	14	712	51	101
11	786	92	1.0359	0.0326	0.1171	0.0023	0.62	0.0642	0.0016	722	23	714	14	747	52	96
12	724	88	1.0670	0.0312	0.1217	0.0024	0.67	0.0636	0.0014	737	22	740	14	728	46	102
13	1024	123	1.0553	0.0338	0.1199	0.0023	0.61	0.0638	0.0016	732	23	730	14	736	54	99
14	524	63	1.0491	0.0316	0.1195	0.0023	0.65	0.0637	0.0015	728	22	728	14	731	49	100
15	341	41	1.0570	0.0311	0.1206	0.0024	0.66	0.0636	0.0014	732	22	734	14	727	47	101
16	367	45	1.0685	0.0312	0.1213	0.0024	0.67	0.0639	0.0014	738	22	738	14	737	46	100

(*continued on next page*)

Table 2 (*continued*)

THMB (pegmatites from the Neno)																
			Ratios							Ages (Ma)						
S no.	U [ppm]	Pb [ppm]	207 Pb/ 235U	±2σ	206 Pb/ 238U	±2σ	rho	207Pb/ 206 Pb	±2σ	207 Pb/ 235U	±2σ	206 Pb/ 238U	±2σ	207Pb/ 206 Pb	±2σ	concordance (%)
17	270	32	1.0629	0.0319	0.1201	0.0024	0.65	0.0642	0.0015	735	22	731	14	749	48	98
18	372	45	1.0542	0.0311	0.1202	0.0024	0.67	0.0636	0.0014	731	22	732	14	728	47	100

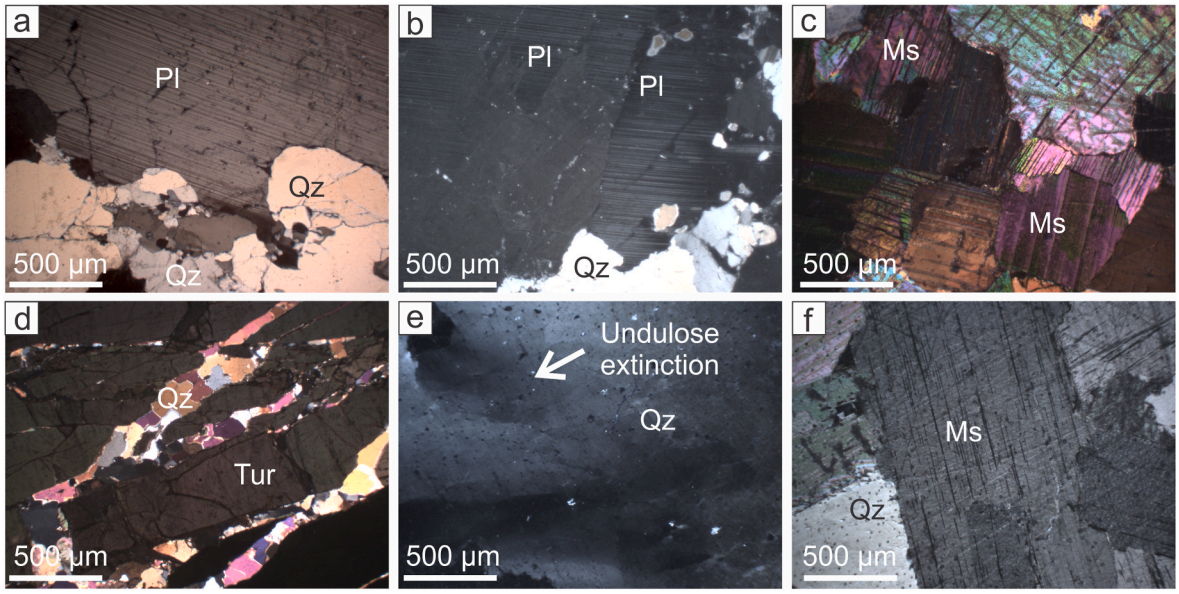

Fig. 4. (a–e) Cross-polarised photomicrographs of thin sections. a) and b) Microstructure of the GWC and GM pegmatites. Plagioclase and quartz show undeformed magmatic textures and no evidence of significant alteration; c) Pegmatitic muscovite of the GM pegmatite with minor undulose extinction but no evidence of alteration or recrystallisation; d) Tourmaline and quartz in the GD pegmatite. Tourmaline shows brittle fractures but no evidence of plastic deformation; e) Large pegmatitic quartz in GNS-1 with undulose extinction and minor subgrain formation, but no evidence of recrystallisation; f) Pegmatitic quartz and muscovite in the GN pegmatite (plane-polarised light).

(Figs. 5a and 6).

4.2.2. *Aquamarine bearing pegmatite: sample GM*

Two muscovite crystals, a K-feldspar crystal and a plagioclase multigrain fraction from the aquamarine bearing pegmatite GM yield a mineral isochron age of 485 ± 5 Ma and a MSWD of 1.03 (Fig. 5b; Table 1). The initial $^{87}Sr/^{86}Sr$ ratio of 0.7762 ± 0.0012 is similarly high as of the GCW pegmatite (Fig. 6).

4.2.3. *Tourmaline pegmatite: sample GD*

Two muscovites from different size fractions and a K-feldspar yield a Rb–Sr mineral isochron age of 489 ± 5 Ma with a good fit of the correlation line (MSWD of 0.41; Fig. 5c). The initial $^{87}Sr/^{86}Sr$ ratio of sample GD is high (0.7405 ± 0.0048; Fig. 5c; Table 1), but lower than the Sr_i ratios of the GM and GCW pegmatites (Fig. 6).

4.2.4. *Tourmaline pegmatites: samples GNS-1 and GNS-4*

The Rb–Sr mineral isochron formed by two muscovite crystals, a K-feldspar and a plagioclase crystal from the pegmatite sample GNS-1 yields an age of 555 ± 5 Ma (Fig. 5d). This pegmatite is thus ~50 m.y. older than the GD, GM and GCW pegmatites from central and northern Malawi. The initial $^{87}Sr/^{86}Sr$ ratio of 0.706067 ± 0.000035 of the GNS-1 pegmatite is significantly lower than in those pegmatites further north (Figs. 1, 5d and 6). Unlike in other samples discussed earlier, the two muscovite crystals in GNS-1 show highly contrasting $^{87}Rb/^{86}Sr$ ratios (Fig. 5a–d). However, both fractions are well aligned on the low-MSWD regression line (MSWD = 2.0, Fig. 5d), indicating initial isotopic equilibrium between all mica and feldspar phases.

A three-point isochron of 552 ± 6 Ma is defined by two muscovite crystal fragments and a K-feldspar multigrain fraction from the pegmatite sample GNS-4 (Fig. 5e). Within the analytical uncertainty, the ages of GNS-1 and GNS-4 are indistinguishable. The Sr_i of 0.70558 ± 0.00062 of GNS-4 is close to the Sr_i of GNS-1 (Figs. 5e and 6).

4.2.5. *Tourmaline-sunstone pegmatite: sample GN*

Rb–Sr data for two muscovite crystals and a K-feldspar fraction define an isochron corresponding to an age of 460 ± 5 Ma (Fig. 5f). The initial $^{87}Sr/^{86}Sr$ ratio is very high, 0.7893 ± 0.0099 (Figs. 5f and 6).

4.2.6. *Amethyst pegmatite: sample GU*

The sample GU provides an age of 520 ± 6 Ma, obtained from a three-point isochron of K-feldspar, plagioclase and biotite multigrain fractions (Fig. 5g). The initial $^{87}Sr/^{86}Sr$ ratio of sample GU is 0.718733 ± 0.000059 (Figs. 5g and 6).

4.3. *U–Pb isotope analysis*

4.3.1. *Zircon bearing pegmatites (Samples MNM and NNO)*

Pegmatite MNM contains euhedral gem-quality zircon up to 30 mm in size. Irregularly shaped cores may indicate either inherited material or may be related to resorption processes in the early growth stage of pegmatitic zircon. However, such domains are overgrown by thick zircon rims with oscillatory patterns that indicate later magmatic growth (Fig. 7a and b).

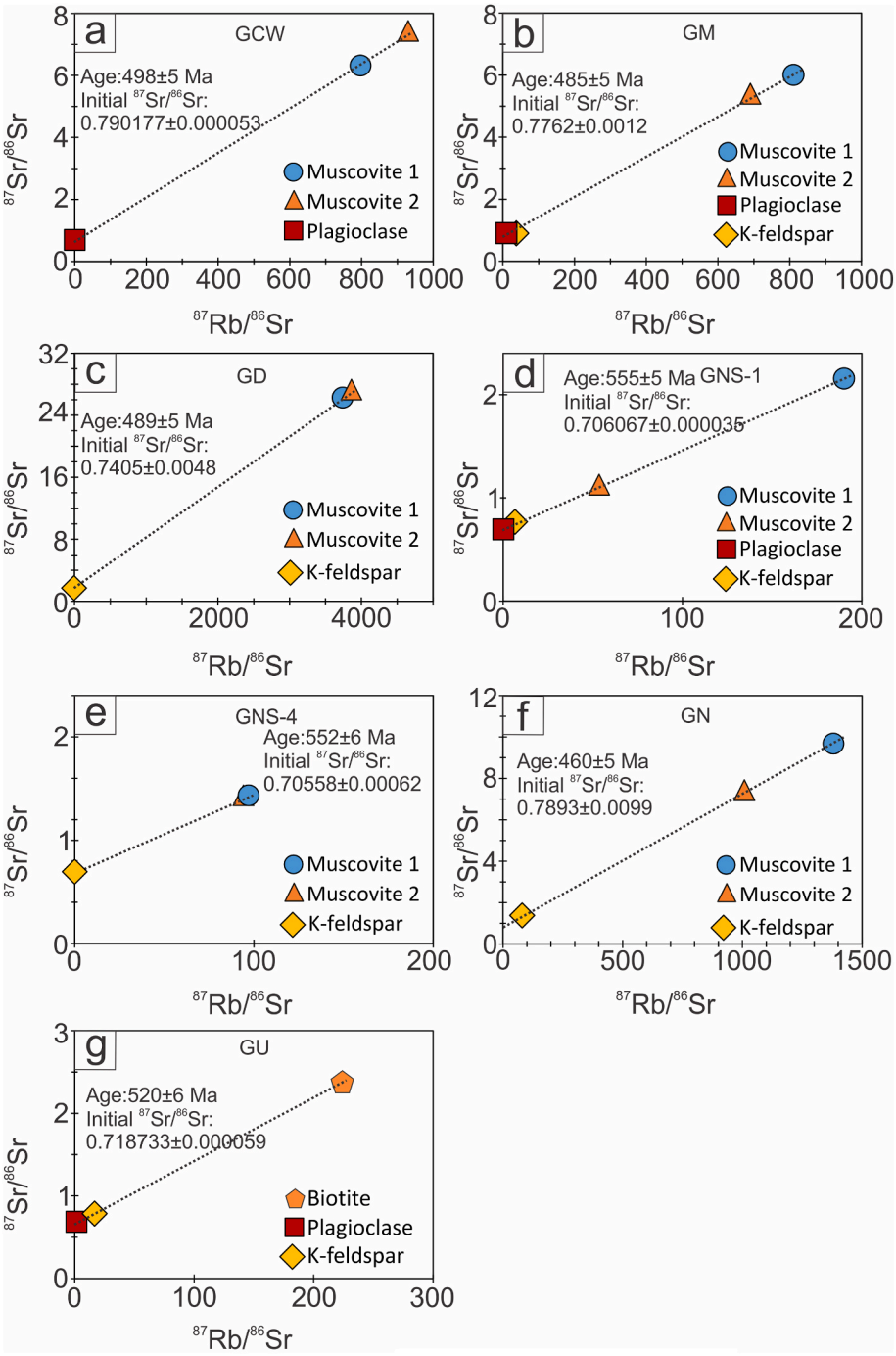

Fig. 5. Rb–Sr isochron diagrams including initial $^{87}Sr/^{86}Sr$ ratios and emplacement ages.

The analysed areas contain between 19 and 153 ppm U with a mean Th/U ratio of 0.2. Thirty spot analyses provided (near-) concordant (94%–102%) analyses, from which a concordant age of 598 ± 15 Ma with MSWD of 0.22 was obtained (Fig. 8a). This age is interpreted as crystallization age of the pegmatitic zircon, and thus as the emplacement age of MNM. The $^{207}Pb/^{206}Pb$ ages range from 585 to 625 Ma (Table 2). The calculated weighted mean $^{206}Pb/^{238}U$ age of these data is 594 ± 3 Ma (Fig. 8b). This excludes two analyses that show significantly older U–Pb and Pb–Pb ages (732–753 Ma). These data were obtained from the core of the zircon (Fig. 7b) and may represent an inherited zircon component from an earlier growth event unrelated to the MNM pegmatite formation.

The zircon crystals in the sample NNO reach up to 20 mm in size and are typically euhedral (Fig. 2f). The CL imagery shows oscillatory patterns indicative of magmatic growth (Fig. 7c). The analysed areas contain between 41 and 615 ppm U with a mean Th/U ratio of 0.35, indicating the igneous origin of zircon (Belousova et al., 2002). A concordant age of 719 ± 5 Ma with MSWD of 0.24 was obtained from eighteen spot analyses (Fig. 8c). This concordant age is interpreted as the pegmatite emplacement age. The $^{207}Pb/^{206}Pb$ ages range from 694 to 749 Ma, whereas the calculated weighted mean $^{206}Pb/^{238}U$ age is 720 ± 6 Ma, overlapping with the concordant U–Pb age (Fig. 8d).

4.3.2. *Zircon bearing pegmatite: sample THMB*

The zircon crystals present in the pegmatite sample from Neno reach up to 35 mm in size and are generally euhedral. The CL imagery reveals

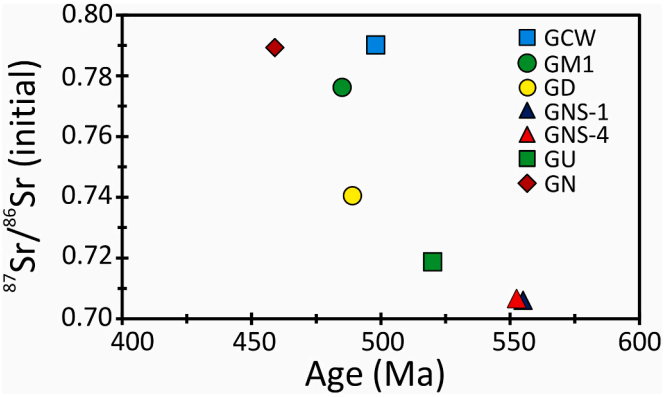

Fig. 6. $^{87}Sr/^{86}Sr$ ratios vs. emplacement ages of pegmatites dated with the Rb–Sr isochron method.

concentric zonation with irregularly shaped areas (Fig. 7d).

The analysed grains contain between 120 and 1100 ppm U with a mean Th/U ratio of 0.5. Eighteen spot analyses with concordant results yield an emplacement age of 729 ± 4 Ma (MSWD is 0.71, Fig. 8e). The weighted mean $^{206}Pb/^{238}U$ age is 731 ± 4 Ma (Fig. 8f), overlapping with the concordant age results. The $^{207}Pb/^{206}Pb$ ages range from 693 to 749 Ma (Table 2).

5. Discussion

5.1. Timing of pegmatite melt intrusion in the host rocks

The oldest pegmatites are the zircon bearing THMB and NNO pegmatites from the southern Malawian Neno and Mangochi districts (Fig. 1). They intruded their Mesoproterozoic host rocks, two-pyroxene granulites, during a late Tonian/early Cryogenian magmatic event, yielding concordant emplacement ages of 729 ± 4 Ma and 719 ± 5 Ma, respectively. Two dates of 746 ± 44 Ma are reported from zircons in the pegmatite sample MNM from the Nankhwali area (Fig. 1, Table 2, Fig. 8a). These ages are interpreted as inherited zircons in younger pegmatite. The pegmatitic zircon in the MNM pegmatite has been dated as Ediacaran, at 598 ± 15 Ma. Accordingly, two separate episodes of zircon bearing pegmatite formation are evident in southern Malawi, one around the Tonian/Cryogenian boundary and one in the Ediacaran Period.

All other pegmatites contain assemblages that are suitable for Rb–Sr mineral isochron geochronology. The muscovite present in the rocks is primary pegmatitic and the K-feldspar crystals do not show evidence of fluid induced dissolution or major ductile deformation of the pegmatitic assemblages (Fig. 4). Furthermore, all phases defining the isochrons show satisfactory initial Sr-isotopic equilibrium. Accordingly, we consider resetting of the Rb–Sr isotope system during post-pegmatitic fluid influx episodes as unlikely, and rejuvenation by deformation-induced partial recrystallisation of pegmatitic phases (Glodny et al., 1998; Eberlei et al., 2015) can be ruled out. The ages also do not represent cooling ages, as protracted diffusion during cooling would inevitably result in higher apparent ages for larger mica grains (with their larger diffusion domain sizes) compared to smaller-sized mica crystals in a given sample (Glodny et al., 2008), which is not observed. Therefore, we interpret all Rb–Sr mineral isochron age results as the emplacement ages of the dated pegmatites.

The Rb–Sr mineral age data set suggests the prolonged or periodic intrusion of pegmatite forming melts into the Mesoproterozoic basement during the main and late stages of the Pan-African orogeny (~600–500 Ma), but extend into the Ordovician, which post-dates the assembly of Gondwana. The earliest of these pegmatites are GNS-1 and -4, in southern Malawi, that were emplaced in the late Ediacaran at ~555 Ma, followed by the Cambrian ~520 Ma GU pegmatite, some 50 km north-east from the GNS pegmatites (Fig. 1).

All remaining pegmatites are of late Cambrian age (GCW in the far north at 498 ± 5 Ma and GD near Lilongwe in central Malawi, at 489 ± 5 Ma), straddle the Cambrian/Ordovician boundary (GM, 485 ± 5 Ma, in northern Malawi) and reach into Mid-Ordovician time (GN in south Malawi, 460 ± 5 Ma). There is no apparent geographical trend in the sequence of pegmatite emplacement in Malawi (Fig. 1).

The available geochronological data point towards a polyphase

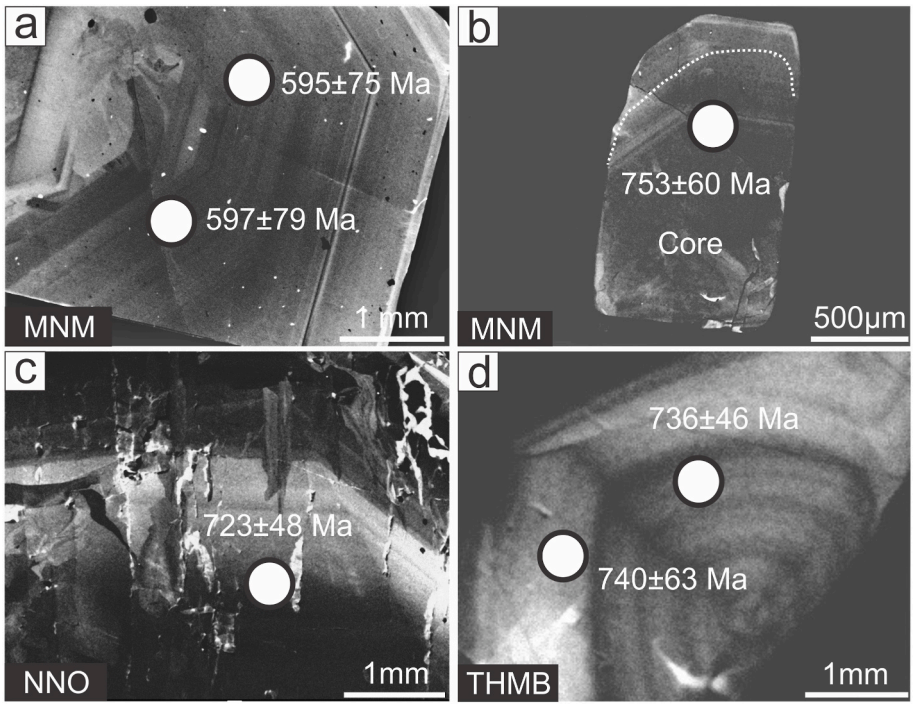

Fig. 7. Cathodoluminescence images of pegmatitic zircon.

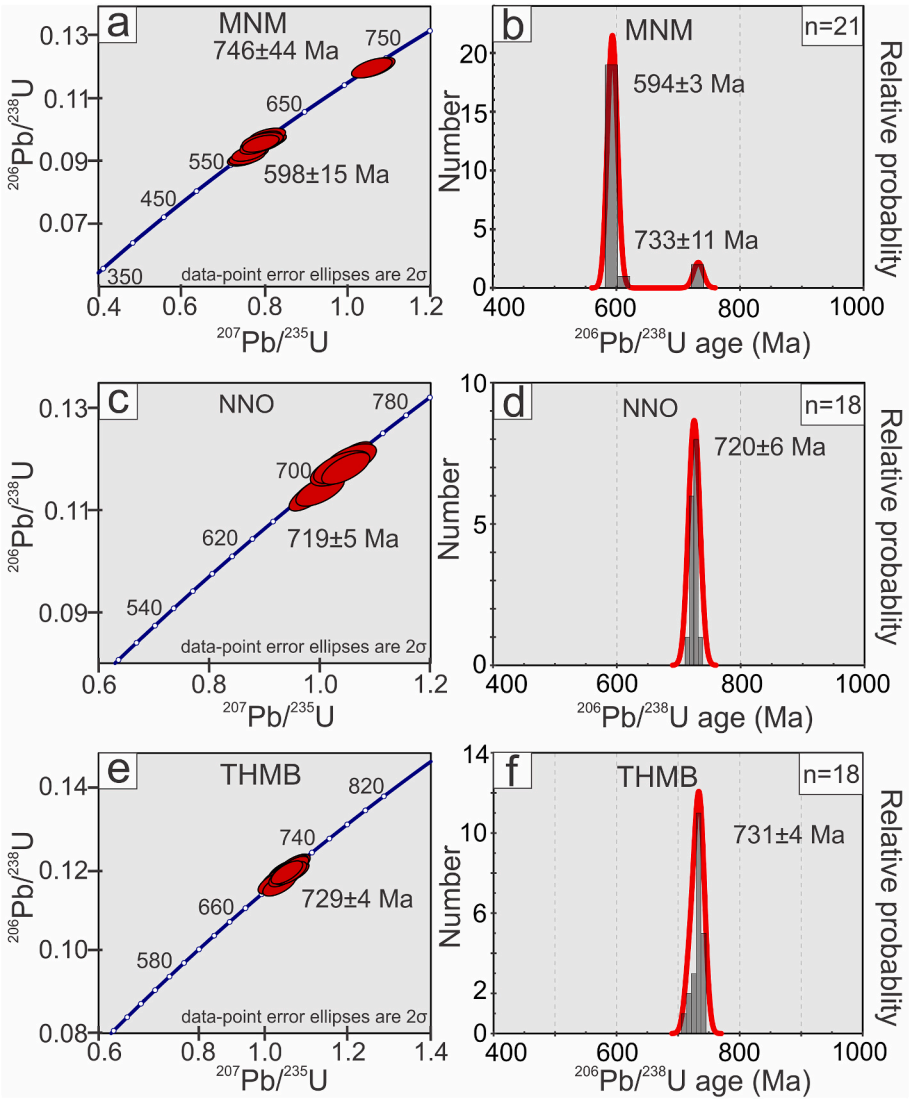

Fig. 8. U–Pb concordia diagrams and $^{206}Pb/^{238}U$ age probability histograms of pegmatitic and inherited zircon.

intrusion of pegmatites into the Malawi gneissic basement throughout the Pan-African orogenic cycle and in post-Pan-African time, over an extended period of 270 million years between ~730 Ma to ~460 Ma. The zircon bearing pegmatites were emplaced early in the Pan-African cycle around 730 Ma, and in a second episode at ~600 Ma. All feldspar- and mica-rich pegmatites, dated using Rb–Sr mineral isochrons, are younger, intruding at ~550–460 Ma.

5.2. Pegmatite sources

The initial Sr isotopic composition of the pegmatites is a useful tool for source identification (Haack and Gohn, 1988; Faure and Mensing, 2005). Usually, high initial Sr isotopic compositions are associated with dominant contributions from old upper crustal material with high Rb/Sr ratios (Spooner and Fairbairn, 1970; Faure and Powell, 1972). The initial Sr isotopic compositions reported in this study show a wide variation between 0.7921 and 0.7060 (Table 1), suggesting a variety of sources.

The comparatively low initial $^{87}Sr/^{86}Sr$ ratios (0.70606–0.70558) observed in the GNS pegmatites imply either a source rock with a low to moderately high Rb/Sr ratio, or a source that had only recently been added to the crust from mantle sources. The ~520 Ma GU pegmatite and the ~489 Ma GD pegmatite show initial $^{87}Sr/^{86}Sr$ ratio of 0.7187and 0.7405, typical of evolved continental crustal sources such as metasedimentary rocks or pre-existing crustal granitoids. The youngest pegmatites, emplaced between ~498 and ~460 Ma (GCW, GM, GN) show initial $^{87}Sr/^{86}Sr$ ratios between 0.7902 and 0.7762, and the melting of typical crustal sources does not sufficiently explain such high initial Sr_i values. There are two possible causes for these values:

1) The pegmatite source was a high-K and initially high Rb, but low-Sr, pelitic or psammopelitic rock that was significantly older than the event that formed the pegmatitic melt. At the time of partial melting such a rock would have been enriched in radiogenic ^{87}Sr, generating S-type granitic magmas with unusually high $^{87}Sr/^{86}Sr$ ratios, from which residual pegmatitic melts may have evolved.
2) Rb–Sr isotopic signatures of primary anatectic melts may depend on the properties of constituent phases of the precursor rock that are involved in the melting reactions (Wolf et al., 2019). Experimental work equally indicates that in granitic systems isotopically distinct melts can arise from progressive melting of a single source (Knesel and Davidson, 2002). The Rb/Sr and $^{87}Sr/^{86}Sr$ ratios in the anatectic melt composition will therefore be controlled by (i) the proportion of mica phases (biotite and muscovite) with their high Rb/Sr, and rapidly evolving $^{87}Sr/^{86}Sr$ ratios in melt formation, (ii) the proportion of major Sr-rich constituents such as Ca-plagioclase, and (iii) the

melting behaviour of particularly Sr-rich accessory phases like apatite (Zeng et al., 2005). Anatectic minimum melts that acquired their Sr and Rb budget mainly from melting of mica phases will therefore have particularly high $^{87}Sr/^{86}Sr$ and Rb/Sr ratios.

The observation that the pegmatites with high initial $^{87}Sr/^{86}Sr$ ratios (GCW, GM, GN) also show extremely high Rb/Sr ratios in their pegmatitic muscovite ($^{87}Rb/^{86}Sr$ generally >500; Table 1) therefore supports pegmatite formation from anatectic minimum melts. This may suggest that these younger pegmatites formed by anatexis rather than granite differentiation, implying a late- or post-orogenic heat pulse affecting the crust in late Cambrian to Mid-Ordovician time.

5.3. Pegmatite emplacement in the context of the Pan-African orogenic cycle

The two oldest pegmatites, emplaced at ~about 725 Ma (THMB and NNO; Figs. 1 and 8), significantly precede the collisional tectonics related to the assembly of Gondwana in East Africa (~600–500 Ma), but post-date the break-up of Rodinia and the formation of the Mozambique Ocean (850–800 Ma; Meert, 2003; Jöns and Schenk, 2008). At the time when THMB and NNO were emplaced, the region of today's Malawi most likely was positioned at the continental margin of Eastern Gondwana along the Mozambique Ocean (Kröner et al., 2001). .

In southern Malawi, and close to the location of the 729 ± 4 Ma THMB pegmatite (Fig. 1), the Tambani alkaline magmatic complex formed at 729 ± 7 Ma and is related to rifting in continental lithosphere (Burke et al., 2003; Ashwal et al., 2007). The NNO pegmatite was emplaced at the same stage of the orogenic evolution (719 ± 5 Ma), but the sample location is more than 200 km northeast of the Tambani complex. Manda et al. (2019) reported the intrusion of a leucocratic granite at ~735 Ma and of charnockitic magma at around ~715 Ma in southern Malawi at locations closer to the NNO pegmatite. These ages also broadly correlate with the formation age of the rift-related North Nyasa Alkaline Province (~750–710 Ma) in central and northern Malawi (Eby et al., 1998). Accordingly, the THMB and NNO pegmatites formed at a time of high heat influx into the lithosphere around ~715–750 Ma, coinciding with alkaline magmatism and rifting of the lithosphere.

Pegmatite MNM from southern Malawi (Fig. 1) was emplaced at 598 ± 15 Ma, which may allow its association either with a waning stage of the East African Orogeny or an early stage of the Kuunga Orogeny. This pegmatite contains significantly older inherited magmatic zircon formed at 746 ± 44 Ma, an age similar to the emplacement ages of the NNO and THMB pegmatites. This indicates crustal recycling and renewed magmatism following the subduction of the Mozambique Ocean and the collision of Eastern and Western Gondwana during the East African Orogeny. However, the emplacement of the MNM pegmatite preceded the peak of Pan-African regional high-temperature metamorphism in southern Malawi, which is forty to eighty million years younger (Ashwal et al., 2007; Bingen et al., 2009).

The GNS pegmatites from Ntcheu (555 ± 5 Ma and 552 ± 6 Ma; Fig. 1) are located between the Luiro Belt and the Mwembeshi shear zone, both of which are associated with the Kuunga Orogeny (Meert, 2003; Grantham et al., 2003, 2019; Viola et al., 2008). The GNS pegmatites also coincide chronologically with the earliest record of Kuunga-related collisional tectonics and high-temperature metamorphism in the Unango and Marrupa complexes of nearby NE Mozambique, which has been dated as ~555 Ma (Melezhik et al., 2006; Bingen et al., 2009) and granite emplacement extending further north into southern Tanzania (~590–550 Ma; Thomas et al., 2014). Accordingly, the GNS pegmatites are chronologically correlated with magmatism during the collisional and high-temperature metamorphic phase of the Kuunga Orogeny.

The tectonic context of the late-Cambrian and Ordovician pegmatites (GCW, GM, GD, GN and GU; 520–460 Ma) is less clear. Crustal thickening and granulite facies metamorphism associated with the Kuunga Orogeny in northern Mozambique and in the Lurio Belt took place at 570–530 Ma (Engvik et al., 2007; Macey et al., 2007, 2010, 2013; Bingen et al., 2009), significantly predating the emplacement of these younger pegmatites. An episode of crustal extension and intrusion of post-collisional granites ranging between 530 and 485 Ma (Macey et al., 2007, 2010, 2013; Jacobs et al., 2008; Bingen et al., 2009; Ueda et al., 2012; Fritz et al., 2013) overlaps in time with the emplacement of the late Cambrian to Ordovician pegmatites GCW, GM, GD, and GU, but not with the 460 ± 5 Ma GN pegmatite. However, we associate all pegmatites that are 520 Ma or younger with the prolonged post-collisional, probably extensional episode in the aftermath of the Kuunga continent collision.

6. Conclusions

The Pan-African orogenic cycle endowed Malawi with abundant gem bearing pegmatites containing zircon, tourmaline, aquamarine, beryl, and other gem species. Gem bearing pegmatites formed at multiple stages throughout the Pan-African cycle. Late Tonian zircon pegmatites, emplaced during rifting of Eastern Gondwana lithosphere were followed by a second episode of Ediacaran (~598 Ma) zircon pegmatite formation in the latest stage of the East African Orogeny. The Kuunga Orogeny and its aftermath appears to be the Pan-African phase in which the formation of gem bearing pegmatites was most productive, with beryl, aquamarine, amethyst, sunstone, and tourmaline as gem mineralization.

The remnant crustal heat from the preceding East African Orogeny may have contributed to higher crustal temperatures at the beginning of the Kuunga-related amalgamation of southern and northern Gondwana, creating more fertile conditions for crustal magmatism around and after ~550 Ma in those regions where the EAO and the Kuunga Orogen overlapped. The abundant formation of pegmatites in Malawi and the neighbouring regions (southern Tanzania, northern Mozambique, eastern Zambia; e.g. Simmons et al., 2012) at that time may be seen in this context.

The large spread of initial $^{87}Sr/^{86}Sr$ ratios in our data set suggests that the pegmatites that were emplaced between ~550 Ma and ~460 Ma formed essentially from crustal but isotopically highly variable sources. The contribution of high-Rb minerals (muscovite, biotite) to melt formation during crustal anatexis is the most likely reason for very high Sr initial isotope ratios that we observe in some of our pegmatites. A late Cambrian or Mid-Ordovician heat pulse forming pegmatites as first anatectic melts is isotopically possible but is not evident from the available literature on the regional geological evolution.

Declaration of competing interest

The authors declare the following financial interests/personal relationships which may be considered as potential competing interests: Tuhin Chakraborty reports financial support was provided by Glencore UK Ltd.

Data availability

We have recorded the data in Table 1 and Table 2.

Acknowledgments

Glencore-Xstrata funded a post-doctoral fellowship for TC. The DST-NRF Centre of Excellence for Integrated Mineral and Energy Resource Analysis (CIMERA) supported funding for analytical costs and provided a partial bursary for CFK's PhD studies. Deon van Niekerk (Rhodes University) is thanked for technical assistance CL-EPMA analysis. The Rhodes University EPMA laboratory was funded by a grant from the NRF National Equipment Programme (UID: 74464). We thank R.E. Hanson, S. Oriolo, R.J. Thomas and an anonymous reviewer for providing helpful

comments on the regional geology in their reviews. We also acknowledge the editorial handling by Mohamed G. Abdelsalam.

Appendix A. Supplementary data

Supplementary data to this article can be found online at https://doi.org/10.1016/j.jafrearsci.2022.104750.

References

Ashwal, L.D., Armstrong, R.A., Roberts, R.J., Schmitz, M.D., Corfu, F., Hetherington, C.J., Burke, K., Gerber, M., 2007. Geochronology of zircon megacrysts from nepheline-bearing gneisses as constraints on tectonic setting: implications for resetting of the U-Pb and Lu-Hf isotopic systems. Contrib. Mineral. Petrol. 153, 389–403. https://doi.org/10.1007/s00410-006-0153-9.

Belousova, E.A., Griffin, W.L., O'Reilly, S.Y., Fisher, N.I., 2002. Igneous zircon: trace element composition as an indicator of source rock type. Contrib. Mineral. Petrol. 1435 143, 602–622. https://doi.org/10.1007/S00410-002-0364-7, 2002.

Bingen, B., Jacobs, J., Viola, G., Henderson, I.H.C., Skår Boyd, R., Thomas, R.J., Solli, A., Key, R.M., Daudi, E.X.F., 2009. Geochronology of the Precambrian crust in the Mozambique belt in NE Mozambique, and implications for Gondwana assembly. Precambrian Res. 170, 231–255. https://doi.org/10.1016/j.precamres.2009.01.005.

Bloomfield, K., 1968. Pre-Karroo Geology of Malawi. Malawi, Geol. Surv, vol. 5. Dept-Memoir, p. 166.

Bloomfield, K., Garson, M.S., 1965. The geology of the Kirk-range-Lisungwe valley area. Bull. Geol. Soc. Malays. 17.

Burke, K., Ashwal, L.D., Webb, S.J., 2003. New way to map old sutures using deformed alkaline rocks and carbonatites. Geology 31, 391–394. https://doi.org/10.1130/0091-7613(2003)031<0391:NWTMOS>2.0.CO;2.

Carranza, E.J.M., Woldai, T., Chikambwe, E.M., 2005. Application of data-driven evidential belief functions to prospectivity mapping for aquamarine-bearing pegmatites, Lundazi district, Zambia. Nat. Resour. Res. 14, 47–63.

Carter, G.S., Bennet, J.D., 1973. The geology and mineral resources of Malawi. Bull. Geol. Soc. Malays. 6.

Collins, A.S., Pisarevsky, S.A., 2005. Amalgamating eastern Gondwana: the evolution of the Circum-Indian orogens. Earth Sci. Rev. 71, 229–270. https://doi.org/10.1016/J.EARSCIREV.2005.02.004.

Cooper, W., Bloomfield, K., 1961. The geology of the Tambani-Salambidwe area (with accompanying geological map, scale 1:100,000). Geol. Surv. Nyasal. Bull. 13, 63.

Daly, M.C., 1986. Crustal shear zones and thrust belts: their geometry and continuity in Central Africa. Phil.-Transactions R. Soc. London A317, 111–128.

Dill, H.G., 2007. A review of mineral resources in Malawi: with special reference to aluminium variation in mineral deposits. J. Afr. Earth Sci. 47, 153–173. https://doi.org/10.1016/J.JAFREARSCI.2006.12.006.

Eberlei, T., Habler, G., Wegner, W., Schuster, R., Körner, W., Thöni, M., Abart, R., 2015. Rb/Sr isotopic and compositional retentivity of muscovite during deformation. Lithos 227, 161–178. https://doi.org/10.1016/J.LITHOS.2015.04.007.

Eby, G.N., Woolley, A.R., Platt, V.D.G., 1998. Geochemistry and petrogenesis of nepheline syenites: Kasungu-Chipala, Ilomba, and Ulindi nepheline syenite intrusions, North Nyasa alkaline province, Malawi. J. Petrol. 39, 1405–1424. https://doi.org/10.1093/petroj/39.8.1405.

Engvik, A.K., Tveten, E., Bingen, B., Viola, G., Erambert, M., Feito, P., De Azavedo, S., 2007. P-T-t evolution and textural evidence for decompression of Pan-African high-pressure granulites, Lurio Belt, north-eastern Mozambique. J. Metamorph. Geol. 25, 935–952. https://doi.org/10.1111/J.1525-1314.2007.00736.X.

Faure, G., Mensing, T.M., 2005. Isotopes : Principles and Applications. Wiley, Hoboken, New Jersey, p. 928.

Faure, G., Powell, J.L., 1972. Strontium Isotope Geology. Springer-Verlag, Berlin, Heidelberg, p. 188.

Fitzsimons, I.C.W., 2016. Pan-African granulites of Madagascar and southern India: Gondwana assembly and parallels with modern Tibet. J. Mineral. Petrol. Sci. 111, 73–88. https://doi.org/10.2465/jmps.151117.

Fitzsimons, I.C.W., Hulscher, B., 2005. Out of Africa: detrital zircon provenance of central Madagascar and Neoproterozoic terrane transfer across the Mozambique Ocean. Terra. Nova 17, 224–235. https://doi.org/10.1111/J.1365-3121.2005.00595.X.

Foster, A., 1965. Der Kristallinsockel im östlichen Nordrhodesien und sein Verband mit anderen Baueinheiten Zentral- and Ostafrikas. Geotekt. Forsch. 20, 115.

Fritz, H., Abdelsalam, M., Ali, K.A., Bingen, B., Collins, A.S., Fowler, A.R., Ghebreab, W., Hauzenberger, C.A., Johnson, P.R., Kusky, T.M., Macey, P., Muhongo, S., Stern, R.J., Viola, G., 2013. Orogen styles in the east African orogen: a review of the Neoproterozoic to Cambrian tectonic evolution. J. Afr. Earth Sci. 86, 65–106. https://doi.org/10.1016/j.jafrearsci.2013.06.004.

Ganbat, A., Tsujimori, T., Boniface, N., Pastor-Galán, D., Aoki, S., Aoki, K., 2021. Crustal evolution of the Paleoproterozoic Ubendian belt (SW Tanzania) western margin: a central African Shield amalgamation tale. Gondwana Res. 91, 286–306. https://doi.org/10.1016/j.gr.2020.12.009.

Gaskell, J.L., 1973. The geology of the Mzimba area. Bull. Geol. Soc. Malays. 37.

Glodny, J., Grauert, B., Fiala, J., Vejnar, Z., Krohe, A., 1998. Metapegmatites in the western Bohemian Massif: ages of crystallisation and metamorphic overprint, as constrained by U–Pb zircon, monazite, garnet, columbite and Rb–Sr muscovite data. Geol. Rundsch. 871 87, 124–134. https://doi.org/10.1007/S005310050194, 1998.

Glodny, J., Kühn, A., Austrheim, H., 2008. Diffusion versus recrystallization processes in Rb–Sr geochronology: isotopic relics in eclogite facies rocks, Western Gneiss Region, Norway. Geochem. Cosmochim. Acta 72 (2), 506–525.

Grantham, G.H., Kramers, J.D., Eglington, B., Burger, E.P., 2019. The Ediacarian-Cambrian uplift history of western dronning Maud Land: new ^{40}Ar-^{39}Ar and Sr/Nd data from Sverdrupfjella and Kirwanveggan, the source of the Urfjell group and tectonic evolution of dronning Maud Land within the Kuunga orogeny and Gondwana amalgamation. Precambrian Res. 333, 105444 https://doi.org/10.1016/J.PRECAMRES.2019.105444.

Grantham, G.H., Maboko, M., Eglington, B.M., 2003. A review of the evolution of the Mozambique Belt and implications for the amalgamation and dispersal of Rodinia and Gondwana. Geol. Soc. Spec. Publ. 206, 401–425. https://doi.org/10.1144/GSL.SP.2003.206.01.19.

Grantham, G.H., Macey, P.H., Ingram, B.A., Roberts, M.P., Armstrong, R.A., Hokada, T., Shiraishi, K., Jackson, C., Bisnath, A., Manhica, V., 2008. Terrane correlation between Antarctica, Mozambique and Sri Lanka; comparisons of geochronology, lithology, structure and metamorphism and possible implications for the geology of southern Africa and Antarctica. Geol. Soc. London, Spec. Publ. 308, 91–119.

Grantham, G.H., Macey, P.H., Horie, K., Kawakami, T., Ishikawa, M., Satish-Kumar, M., Tsuchiya, N., Graser, P., Azevedo, S., 2013. Comparison of the metamorphic history of the Monapo complex, northern Mozambique and Balchenfjella and Austhameren areas, Sør Rondane, Antarctica: implications for the Kuunga orogeny and the amalgamation of N and S. Gondwana. Precambrian Res. 234, 85–135. https://doi.org/10.1016/J.PRECAMRES.2012.11.012.

Graziani, G., Gubelin, E., Lucchesi, S., 1983. The Genesis of an Emerald from the Kitwe District, Zambia. N Jb. Miner. Mh, pp. 175–186.

Haack, U., Gohn, E., 1988. Rb-Sr data on some pegmatites in the Damara Orogen, Namibia. Commun. Geol. Surv. SWA/Namibia 4, 13–17.

Hanson, R.E., 2003. Proterozoic geochronology and tectonic evolution of southern Africa. Geol. Soc. Spec. Publ. 206, 427–463. https://doi.org/10.1144/GSL.SP.2003.206.01.20.

Harris, J.F., 1981. Summary of the geology of Tanganyika. Part IV Econ. Geol. Tanganyika, Mem. 1, 143.

Holt, D.N., 1965. The Kangankunde Hill rare earth prospect. Bull. Geol. Soc. Malays. 20.

Jacobs, J., Bingen, B., Thomas, R.J., Bauer, W., Wingate, M.T.D., Feitio, P., 2008. Early Palaeozoic orogenic collapse and voluminous late-tectonic magmatism in Dronning Maud Land and Mozambique: insights into the partially delaminated orogenic root of the East African-Antarctic Orogen? Geol. Soc. Spec. Publ. 308, 69–90. https://doi.org/10.1144/SP308.3.

Jöns, N., Schenk, V., 2008. Relics of the Mozambique ocean in the central East African orogen: evidence from the Vohibory block of southern Madagascar. J. Metamorph. Geol. 26, 17–28. https://doi.org/10.1111/j.1525-1314.2007.00745.x.

King, A., Dawson, A., 1976. The geology of the Mangochi-Makanjira area. Bull. Geol. Soc. Malays. 35.

Klerkx, J., Theunissen, K., Delvaux, D., 1998. Persistent fault controlled basin formation since the Proterozoic along the western Branch of the east African rift. J. Afr. Earth Sci. 26, 347–361.

Knesel, K.M., Davidson, J.P., 2002. Insights into collisional magmatism from isotopic fingerprints of melting reactions. Science 296, 2206–2208. https://doi.org/10.1126/SCIENCE.1070622.

Kröner, A., Willner, A.P., Hegner, E., Jaeckel, P., Nemchin, A., 2001. Single zircon ages, PT evolution and Nd isotopic systematics of high-grade gneisses in southern Malawi and their bearing on the evolution of the Mozambique Belt in southeastern Africa. Precambrian Res. 109, 257–291. https://doi.org/10.1016/S0301-9268(01)00150-4.

Lawver, L., Gahagan, L., Dalziel, I., 1998. A tight fit-early Mesozoic Gondwana, a plate reconstruction perspective. Mem. Natl. Inst. Polar Res. 53, 214–229.

Lenoir, J.L., Liegeois, J.P., Theunissen, K., Klerkx, J., 1994. The Paleoproterozoic Ubendian shear belt in Tanzania: geochronology and structure. J. Afr. Earth Sci. 19 (3), 169–184. https://doi.org/10.1016/0899-5362(94)90059-0.

Li, Z.X., Bogdanova, S.V., Collins, A.S., Davidson, A., De Waele, B., Ernst, R.E., Fitzsimons, I.C.W., Fuck, R.A., Gladkochub, D.P., Jacobs, J., Karlstrom, K.E., Lu, S., Natapov, L.M., Pease, V., Pisarevsky, S.A., Thrane, K., Vernikovsky, V., 2008. Assembly, configuration, and break-up history of Rodinia: a synthesis. Precambrian Res. 160, 179–210. https://doi.org/10.1016/j.precamres.2007.04.021.

Macey, P.H., Miller, J.A., Rowe, C.D., Grantham, G.H., Siegfried, P., Armstrong, R.A., Kemp, J., Bacalau, J., 2013. Geology of the Monapo Klippe, NE Mozambique and its significance for assembly of central Gondwana. Precambrian Res. 233, 259–281. https://doi.org/10.1016/j.precamres.2013.03.012.

Macey, P.H., Ingram, B.A., Cronwright, M.S., Botha, G.A., Roberts, M.R., Grantham, G. H., Maree, L.P., Botha, P.M.W., Kota, M., Opperman, R., Haddon, I.G., Nolte, J.C., Rower, M., 2007. Map Explanation Sheets Alto Molócuè (1537), Murrupula (1538), Nampula (1539), Mogincual (1540), Errego (1637), Gilé (1638), and Angoche (1639–40). National Directorate of Geology, Republic of Mozambique.

Macey, P.H., Thomas, R.J., Grantham, G.H., Ingram, B.A., Jacobs, J., Armstrong, R.A., Roberts, M.P., Bingen, B., Hollick, L., de Kock, G.S., Viola, G., Bauer, W., Gonzales, E., Bjerkgård, T., Henderson, I.H.C., Sandstad, J.S., Cronwright, M.S., Harley, S., Solli, A., Nordgulen, T., Motuza, G., Daudi, E., Manhiça, V., 2010. Mesoproterozoic geology of the Nampula block, northern Mozambique: Tracing fragments of Mesoproterozoic crust in the heart of Gondwana. Precambrian Res. 182, 124–148. https://doi.org/10.1016/J.PRECAMRES.2010.07.005.

Malisa, E., Muhongo, S., 1990. Tectonic setting of gemstone mineralization in the Proterozoic metamorphic terrane of the Mozambique Belt in Tanzania. Precambrian Res. 46, 167–176. https://doi.org/10.1016/0301-9268(90)90071-W.

Manda, B.W.C., Cawood, P.A., Spencer, C.J., Prave, T., Robinson, R., Roberts, N.M.W., 2019. Evolution of the Mozambique Belt in Malawi constrained by granitoid U-Pb,

Sm-Nd and Lu-Hf isotopic data. Gondwana Res. 68, 93–107. https://doi.org/10.1016/j.gr.2018.11.004.
McConnell, R.B., 1950. Outline of the geology of Ufipa and Ubende. Geol. Surv. Tanganyika. Bull. 19.
Meert, J.G., 2003. A synopsis of events related to the assembly of the Eastern Gondwana. Tectonophysics. https://doi.org/10.1016/S0040-1951(02)00629-7.
Melezhik, V.A., Kuznetsov, A.B., Fallick, A.F., Smith, R.A., Gorokhov, I.M., Jamal, D., Catuane, F., 2006. Depositional environments and an apparent age for the Geci meta-limestones: constraints on the geological history of northern Mozambique. Precambrian Res. 148, 19–31. https://doi.org/10.1016/J.PRECAMRES.2006.03.003.
Muhongo, S., 1999. Anatomy of the Mozambique belt of eastern and southern Africa: evidence from Tanzania. Gondwana Res. 2, 369–375. https://doi.org/10.1016/S1342-937X(05)70276-8.
Neiva, A.M.R., 2013. Micas, feldspars and columbite–tantalite minerals from the zoned granitic lepidolite-subtype pegmatite at Namivo, Alto Ligonha, Mozambique. Eur. J. Mineral 25, 967–985. https://doi.org/10.1127/0935-1221/2013/0025-2335.
Oriolo, S., Oyhantçabal, P., Wemmer, K., Siegesmund, S., 2017. Contemporaneous assembly of Western Gondwana and final Rodinia break-up: implications for the supercontinent cycle. Geosci. Front. 8, 1431–1445. https://doi.org/10.1016/j.gsf.2017.01.009.
Oriolo, S., Schulz, B., Geuna, S., Gozález, P.D., Otamendi, J.E., Sláma, J., Druguet, E., Siegesmund, S., 2021. Early Paleozoic accretionary orogens along the western Gondwana margin. Geosci. Front. 12, 109–130. https://doi.org/10.1016/j.gsf.2020.07.001.
Ray, G.E., 1974. The structural and metamorphic geology of northern Malawi. J. Geol. Soc. London. 130, 427–440. https://doi.org/10.1144/GSJGS.130.5.0427.
Reeves, C.V., de Wit, M.J., Sahu, B.K., 2004. Tight reassembly of Gondwana exposes Phanerozoic shears in Africa as global tectonic players. Gondwana Res. 7, 7–19. https://doi.org/10.1016/S1342-937X(05)70302-6.
Simmons, W., Pezzotta, F., Shigley, J., Beurlen, H., 2012. Granitic pegmatites as sources of coloured gemstones. Elements 8, 281–287.
Simonet, C., Okundi, S., Masai, P., 2000. General setting of coloured gemstone deposits in the Mozambique Belt of Kenya – Preliminary considerations. In: Proceedings 9th Conference of the. Geological Society of Kenya, Nairobi, Kenya, pp. 123–138.
Smirmov, V., Pentelkov, V., Tolochko, V., Trifan, M., Zhukov, S., 1973. Geology and minerals of the central part of the Western Rift. Geol. Surv. Tanzania, Rep. Geol. Mapp. 333.
Sommer, H., Kröner, A., 2019. Igneous petrology, zircon geochronology and geochemistry of multiply emplaced granitoid bodies from the Palaeoproterozoic Usagaran domain in central Tanzania. J. Afr. Earth Sci. 150, 626–656. https://doi.org/10.1016/j.jafrearsci.2018.09.017.
Spooner, C.M., Fairbairn, H.W., 1970. Strontium 87/strontium 86 initial ratios in pyroxene granulite terranes. J. Geophys. Res. 75, 6706–6713. https://doi.org/10.1029/JB075I032P06706.
Stern, R.J., 1994. Arc Assembly and Continental Collision in the Neoproterozoic East African Orogen: Implications for the Consolidation of Gondwanaland, pp. 319–351. https://doi.org/10.1146/annurev.ea.22.050194.001535 22.
Sutton, J., Watson, J., James, T., 1954. A study of the metamorphic rocks of Karema and Kungwe Bay, western Tanganyika. Geol. Surv. Tanganyika, Bull. 22, 70.
Thomas, R.J., Bushi, A.M., Roberts, N.M.W., Jacobs, J., 2014. Geochronology of granitic rocks from the Ruangwa region, southern Tanzania - Links with NE Mozambique and beyond. J. Afr. Earth Sci. 100, 70–80. https://doi.org/10.1016/j.jafrearsci.2014.06.012.
Tsunogae, T., Uthup, S., Nyirongo, M.W., Takahashi, K., Rahman, Md.S., Liu, Q., Takamura, Y., Tsutsumi, Y., 2021. Neoproterozoic crustal growth in southern Malawi: new insights from petrology, geochemistry, and U–Pb zircon geochronology, and implications for the Kalahari Craton–Congo Craton amalgamation. Precambrian Res. 352, 106007 https://doi.org/10.1016/j.precamres.2020.106007.
Ueda, K., Jacobs, J., Thomas, R.J., Kosler, J., Jourdan, F., Matola, R., 2012. Delamination-induced late-tectonic deformation and high-grade metamorphism of the Proterozoic Nampula Complex, northern Mozambique. Precambrian Res. 196–197, 275–294. https://doi.org/10.1016/J.PRECAMRES.2011.05.012.
Viola, G., Hendersen, I.H.C., Bingen, B., Thomas, R.J., Smethurst, M.A., de Azavedo, S., 2008. Growth and collapse of a deeply eroded orogen: insights from structural and geochronological constraints on the Pan-African evolution of NE Mozambique. Tectonics 27, TC5009. https://doi.org/10.1029/2008TC002284.
Walshaw, R.D., 1965. The geology of the Ntcheu-Balaka area. Bull. Geol. Soc. Malays. 19.
Whitney, D.L., Evans, B.W., 2010. Abbreviations for names of rock-forming minerals. Am. Mineral. 95, 185–187. https://doi.org/10.2138/am.2010.3371.
Wolf, M., Romer, R.L., Glodny, J., 2019. Isotope disequilibrium during partial melting of metasedimentary rocks. Geochem. Cosmochim. Acta 257, 163–183. https://doi.org/10.1016/j.gca.2019.05.008.
Zeng, L., Asimow, P.D., Saleeby, J.B., 2005. Coupling of anatectic reactions and dissolution of accessory phases and the Sr and Nd isotope systematics of anatectic melts from a metasedimentary source. Geochem. Cosmochim. Acta 69, 3671–3682. https://doi.org/10.1016/j.gca.2005.02.035.